PAPER

Characteristic Comparison between Electric Currents on Upper and Lower Surfaces of Patch Conductor in a Microstrip Antenna

Takafumi FUJIMOTO[†a)], **Kazumasa TANAKA**[††], ***and*** **Mitsuo TAGUCHI**[††], ***Members***

SUMMARY The electric currents on the upper, lower and side surfaces of the patch conductor in a circular microstrip antenna are calculated by using the integral equation method and the characteristic between the electric currents on the upper and lower surfaces is compared. The integral equation is derived from the boundary condition that the tangential component of the total electric field due to the electric currents on the upper, lower and side surfaces of the patch conductor vanishes on the upper, lower and side surfaces of the patch conductor. The electric fields are derived by using Green's functions in a layered medium due to a horizontal and a vertical electric dipole on those surfaces. The result of numerical calculation shows that the electric current on the lower surface is much bigger than that on the upper surface and the input impedance of microstrip antenna depends on the electric current on the lower surface.

key words: *microstrip antenna, integral equation method, Green's function in layered medium, electric currents, input impedance*

1. Introduction

In the analysis of a microstrip antenna (MSA) by the integral equation method [1], [2], the patch conductor of the MSA is assumed to be infinitely thin and the total electric current on the upper and lower surfaces of the patch conductor is derived. However, since the thickness of the real patch conductor is finite, the electric currents flow on the upper, lower and side surfaces of the patch conductor separately.

The authors have analyzed MSAs by using the cavity model [3]–[5]. In the cavity model, the MSA is divided into two regions. The one is the inside region of the cavity which is bounded above and below by the conducting plates and on the side by the admittance wall. The other is the outside region of the cavity. Although the electric current exists on the upper surface of the patch conductor in the outside region of the cavity, the electric current on the upper surface was neglected in the cavity model. In [3]–[5], however, the calculated input impedances agreed well with the measured data. The authors estimated that the electric current on the upper surface of the patch conductor didn't influence the input impedance of the MSA.

The electric currents on the upper, lower and side surfaces of the patch conductor haven't been investigated to the authors' knowledge. For the improvement of the antenna performance and the design of antenna for new applications, it is important to understand the accurate electric current distributions and characteristics. Moreover, when an assumption and approximation are used in the theoretical analysis of the antennas, some reason is needed. The validity of a treatment of the electric current on the upper surface in the cavity model can be proved by deriving the electric current distributions on the upper, lower and side surfaces.

In this paper, the electric currents on the upper, lower and side surfaces of the patch conductor in a circular MSA are derived by using the integral equation method and the characteristic between the electric currents on the upper and lower surfaces is compared. The integral equation is derived from the boundary condition that the tangential component of the total electric field due to the electric currents on the upper, lower and side surfaces of the patch conductor vanishes on those surfaces of the patch conductor. In the conventional integral equation method [1], [2], Green's functions produced by a horizontal electric dipole in a layered medium are used. However, the electric current on the side surface flows to the vertical direction. In this paper, therefore, Green's functions produced by a horizontal and a vertical electric dipole in the layered medium are used. Green's functions in the spectral domain are derived by the boundary conditions at the interfaces between the free space, dielectric and ground plane and the radiation condition. Scalar potentials of point charges associated with the horizontal and vertical electric dipoles are in general different [6]. Mixed-potential integral equation available for such case has been proposed by Michalski et al. [7]. In [7], the mixed-potential integral equation has been derived by introducing the vector potential which comprises the additional vector function called "correction term." In this paper, the mixed-potential integral equation for an arbitrarily shaped conductor in the layered medium proposed by Michalski et al. is applied to the circular MSA to derive the electric currents on the upper, lower and side surfaces of the patch conductor.

In order to investigate the effects of the electric currents on the upper, lower and side surfaces to the input impedances of the MSA, the input impedances due to those electric currents are calculated.

2. Mixed-Potential Integral Equation

Figure 1 shows the geometry of a circular MSA and its coordinate system. The radius and thickness of the circular patch

Manuscript received May 13, 2004.
Manuscript revised September 1, 2004.

[†]The author is with the Division of System Science, Graduate School of Science and Technology, Nagasaki University, Nagasaki-shi, 852-8521 Japan.
[††]The authors are with the Department of Electrical and Electronic Engineering, Faculty of Engineering, Nagasaki University, Nagasaki-shi, 852-8521 Japan.
a) E-mail: takafumi@net.nagasaki-u.ac.jp

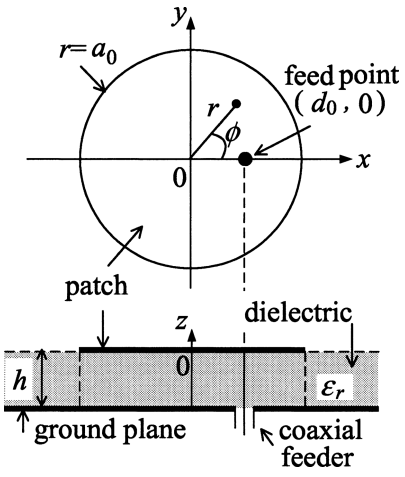

Fig. 1 Geometry of circular microstrip antenna.

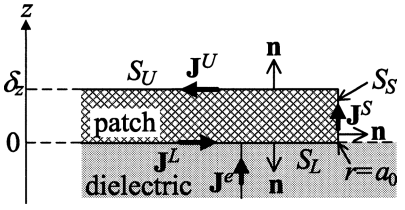

Fig. 2 Electric current distributions on the surfaces of the patch conductor.

conductor are a_0 and δ_z, respectively. The relative dielectric constant and thickness of the dielectric substrate are ε_r and h, respectively. The antenna is excited at $r = d_0$, $\phi = 0°$ by a coaxial feeder through the dielectric substrate.

Figure 2 shows the electric current distributions on the surfaces of the patch conductor. The electric currents on the upper, lower and side surfaces of the patch conductor are denoted by $\mathbf{J}^U$, $\mathbf{J}^L$ and $\mathbf{J}^S$, respectively. In the case of the thin patch conductor, the electric currents on the surfaces of the patch conductor follow closely the behavior of the corresponding eigenmode within the cavity bounded above and below by the conducting plates and on the side by the admittance wall [3]. Therefore, $\mathbf{J}^U$, $\mathbf{J}^L$ and $\mathbf{J}^S$ are expressed as

$$\begin{aligned}\mathbf{J}^{U,L} &= J_r^{U,L}\mathbf{i}_r + J_\phi^{U,L}\mathbf{i}_\phi \\ &= \sum_{m=0}^{M}\sum_{n=0}^{N} A_{mn}^{U,L} F_{rmn}^{U,L}(r,\phi)\mathbf{i}_r \\ &\quad + \sum_{m=0}^{M}\sum_{n=1}^{N} B_{mn}^{U,L} F_{\phi mn}^{U,L}(r,\phi)\mathbf{i}_\phi \end{aligned} \tag{1}$$

$$F_{rmn}^{U,L} = U_m\left(\frac{r}{a_0}\right)\left\{1-\left(\frac{r}{a_0}\right)^2\right\}^{\nu^{U,L}}\cos(n\phi), \quad m+n = \text{even} \tag{2}$$

$$F_{\phi mn}^{U,L} = T_m\left(\frac{r}{a_0}\right)\left\{1-\left(\frac{r}{a_0}\right)^2\right\}^{\nu^{U,L}-1}\sin(n\phi), \quad m+n = \text{odd} \tag{3}$$

$$\begin{aligned}\mathbf{J}^S &= J_z^S\mathbf{i}_z + J_\phi^S\mathbf{i}_\phi \\ &= \sum_{m=0}^{M}\sum_{n=0}^{N} A_{mn}^S F_{zmn}^S(\phi,z)\mathbf{i}_z \\ &\quad + \sum_{m=0}^{M}\sum_{n=1}^{N} B_{mn}^S F_{\phi mn}^S(\phi,z)\mathbf{i}_\phi \end{aligned} \tag{4}$$

$$F_{zmn}^S = U_m\left(\left|1-\frac{2z}{\delta_z}\right|\right)\left\{1-\left(1-\frac{2z}{\delta_z}\right)^2\right\}^{\nu^S} \times\cos(n\phi), \quad m+n = \text{even} \tag{5}$$

$$F_{\phi mn}^S = T_m\left(\left|1-\frac{2z}{\delta_z}\right|\right)\left\{1-\left(1-\frac{2z}{\delta_z}\right)^2\right\}^{\nu^S-1} \times\sin(n\phi), \quad m+n = \text{odd} \tag{6}$$

where ν^S is assumed to be equal to ν^U for $\delta_z/2 \leqq z \leqq \delta_z$ and ν^L for $0 \leqq z \leqq \delta_z/2$. T_n and U_n are Chebyshev polynomials of the first and second kinds, respectively. $\mathbf{i}_r$, $\mathbf{i}_\phi$ and $\mathbf{i}_z$ are unit vectors of the cylindrical coordinate system (r, ϕ, z). $\{A_{mn}^p\}$ and $\{B_{mn}^p\}(p = U, L, S)$ are unknown coefficients. Since the electric currents must be continuous at the center $(x = 0, y = 0)$ of the circular patch conductor, the sums of m and n with respect to the r and ϕ components of the electric currents are even and odd, respectively. The edge conditions of the metallic 90° corner are used. Therefore, ν^U is 0.667 and ν^L is 0.603 for $\varepsilon_r = 2.15$ [8].

The electric fields on the upper, lower and side surfaces of the patch conductor produced by $\mathbf{J}^p(p = U, L, S)$ are denoted by $\mathbf{E}^U(\mathbf{J}^p)$, $\mathbf{E}^L(\mathbf{J}^p)$ and $\mathbf{E}^S(\mathbf{J}^p)$, respectively. The excitation fields on the upper, lower and side surfaces of the patch conductor due to the feed current $\mathbf{J}^e$ are denoted by $\mathbf{E}^U(\mathbf{J}^e)$, $\mathbf{E}^L(\mathbf{J}^e)$ and $\mathbf{E}^S(\mathbf{J}^e)$, respectively. The boundary conditions on the upper, lower and side surfaces of the patch conductor are expressed as

$$\left\{\sum_{p=U,L,S}\mathbf{E}^q(\mathbf{J}^p) + \mathbf{E}^q(\mathbf{J}^e)\right\}\times\mathbf{n} = \mathbf{0} \quad \text{on } S_q,\ q = U, L, S, \tag{7}$$

where $\mathbf{n}$ is the unit normal vector directed outward from the patch conductor and S_U, S_L and S_S are the upper, lower and side surfaces of the patch conductor, respectively (See Fig. 2).

In the formulation of the electric fields, the local coordinate system (X, Y, Z) with the origin located at the point $(r', \phi', -h)$ is used. The prime denotes the source points. Figure 3 shows the local coordinate system (X, Y, Z). The positive X direction is defined by the tangential ϕ' direction. $\mathbf{E}^q(\mathbf{J}^p)$ is expressed by the vector potential $\mathbf{A}^q(\mathbf{J}^p)$ and the scalar potential $\phi_e^q(\mathbf{J}^p)$;

$$\mathbf{E}^q(\mathbf{J}^p) = -j\omega\mathbf{A}^q(\mathbf{J}^p) - \nabla\phi_e^q(\mathbf{J}^p). \tag{8}$$

Since both horizontal and vertical electric dipoles exist in a layered medium, the vector potential $\mathbf{A}^q(\mathbf{J}^p)$ is written as follows [7],

$$\mathbf{A}^q(\mathbf{J}^p) = \int_{S_p} \overline{\overline{\mathbf{K}}}_A \cdot \mathbf{J}^p dS' \tag{9}$$

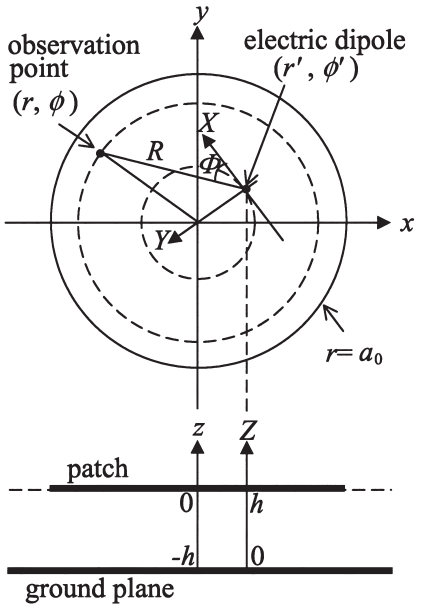

Fig. 3 Local coordinate system (X, Y, Z).

$$\overline{\overline{\mathbf{K}}}_A = \overline{\overline{\mathbf{G}}}_A + \nabla \mathbf{P} \tag{10}$$

where $\overline{\overline{\mathbf{G}}}_A$ is dyadic Green's function and vector function $\mathbf{P}$ is called correction term in [7]. In terms of Sommerfeld potential [1], the dyadic Green's function $\overline{\overline{\mathbf{G}}}_A$ is expressed as follows,

$$\begin{aligned}\overline{\overline{\mathbf{G}}}_A &= (\mathbf{i}_X G_A^{XX} + \mathbf{i}_Z G_A^{ZX})\mathbf{i}_X \\ &\quad + (\mathbf{i}_Y G_A^{YY} + \mathbf{i}_Z G_A^{ZY})\mathbf{i}_Y + \mathbf{i}_Z G_A^{ZZ}\mathbf{i}_Z\end{aligned} \tag{11}$$

where G_A^{ST} is the S component of Green's function for the vector potential due to a T- directed electric dipole. $\mathbf{i}_X$, $\mathbf{i}_Y$ and $\mathbf{i}_Z$ are unit vectors of the local coordinate system (X, Y, Z). The components of the dyadic function $\overline{\overline{\mathbf{K}}}_A$ are expressed by using the components of the dyadic Green's function $\overline{\overline{\mathbf{G}}}_A$ and the vector function $\mathbf{P}$.

$$K_A^{XX} = G_A^{XX} \tag{12}$$
$$K_A^{ZX} = G_A^{ZX} \tag{13}$$
$$K_A^{YY} = G_A^{YY} \tag{14}$$
$$K_A^{ZY} = G_A^{ZY} \tag{15}$$
$$K_A^{XZ} = \frac{\partial P_Z}{\partial X} \tag{16}$$
$$K_A^{YZ} = \frac{\partial P_Z}{\partial Y} \tag{17}$$
$$K_A^{ZZ} = G_A^{ZZ} + \frac{\partial P_Z}{\partial Z} \tag{18}$$

The scalar potential $\phi_e^q(\mathbf{J}^p)$ due to $\mathbf{J}^p$ is written as follows [7],

$$\begin{aligned}\phi_e^q(\mathbf{J}^p) &= -\frac{1}{j\omega}\int_{S_p} G_U(\nabla' \cdot \mathbf{J}^p)dS' \\ &\quad -\frac{1}{j\omega}\int_C G_U J_z^S dl'\end{aligned} \tag{19}$$

where G_U is Green's function for the scalar potential. ∇' is the derivative operator at the source point. C is the contour formed by the intersection of the surface S_S with the interface at $Z = h$. Since $J_z^S = 0$ at $Z = h$, the second term in the right side of Eq. (19) vanishes.

By substituting Eqs. (8), (9) and (19) into Eq. (7), the integral equation is obtained.

$$\begin{aligned}\mathbf{n} \times \sum_{p=U,L,S} \Bigg\{ & j\omega \int_{S_p} \overline{\overline{\mathbf{K}}}_A \cdot \mathbf{J}^p dS' \\ & -\frac{1}{j\omega}\nabla \int_{S_p} G_U(\nabla' \cdot \mathbf{J}^p)dS' \Bigg\} = \mathbf{n} \times \mathbf{E}^q(\mathbf{J}^e)\end{aligned} \tag{20}$$

$\{A_{mn}^p\}$ and $\{B_{mn}^p\}$ are determined by applying the method of moment to the integral equation (20).

The coaxial feeder is assumed to be an infinitely thin filament whose end is connected to the patch conductor at its lower surface. Therefore, the feed current $\mathbf{J}_e$ entering the point $(r = d_0, \phi = 0°)$ is given by a product of Dirac's delta functions.

$$\mathbf{J}^e = \frac{\delta(r - d_0)\delta(\phi)}{r}\mathbf{i}_z \quad (-h \leqq z \leqq 0) \tag{21}$$

The matrix elements with respect to the excitation fields in the matrix equation can be calculated using the reciprocity theorem [1].

3. Green's Functions in the Spectral Domain

The Z component of the electric and magnetic fields created by the T-directed electric dipole are denoted by G_E^{ZT} and G_H^{ZT}, respectively. Using the notation "-" for the quantity in the spectral domain, $\overline{G}_A^{XX}$, $\overline{G}_A^{ZX}$, $\overline{G}_A^{YY}$, $\overline{G}_A^{ZY}$, $\overline{G}_A^{ZZ}$, $\overline{P}_Z$ and $\overline{G}_U$ are expressed as [1], [7],

$$\overline{G}_A^{XX} = \overline{G}_A^{YY} = -\frac{\mu_0}{jk_Y}\overline{G}_H^{ZX} \tag{22}$$

$$\overline{G}_A^{ZX} = \frac{j\omega\mu_0\varepsilon_i}{{k_R}^2}\overline{G}_E^{ZX} + \frac{\mu_0 k_X}{{k_R}^2 k_Y}\frac{\partial \overline{G}_H^{ZX}}{\partial Z} \tag{23}$$

$$\overline{G}_A^{ZY} = \frac{j\omega\mu_0\varepsilon_i}{{k_R}^2}\overline{G}_E^{ZY} - \frac{\mu_0 k_Y}{{k_R}^2 k_X}\frac{\partial \overline{G}_H^{ZY}}{\partial Z} \tag{24}$$

$$\overline{G}_A^{ZZ} = \frac{j\omega\mu_0\varepsilon_i}{{k_R}^2}\overline{G}_E^{ZZ} \tag{25}$$

$$\begin{aligned}\overline{P}_Z = \frac{1}{{k_i}^2}\Bigg(& -\frac{\mu_0}{jk_Y}\frac{\partial \overline{G}_H^{ZX}}{\partial Z'} + \frac{\omega\mu_0\varepsilon_i}{{k_R}^2 k_X}\frac{\partial^2 \overline{G}_E^{ZX}}{\partial Z' \partial Z} \\ & + \frac{\mu_0}{j{k_R}^2 k_Y}\frac{\partial^3 \overline{G}_H^{ZX}}{\partial Z' \partial Z^2} + \frac{j\omega\mu_0\varepsilon_i}{{k_R}^2}\frac{\partial \overline{G}_E^{ZZ}}{\partial Z}\Bigg)\end{aligned} \tag{26}$$

$$\overline{G}_U = \frac{\omega}{k_X {k_R}^2}\frac{\partial \overline{G}_E^{ZX}}{\partial Z} - \frac{{k_i}^2}{jk_Y\varepsilon_i {k_R}^2}\overline{G}_H^{ZX} \tag{27}$$

$${u_i}^2 = {k_R}^2 - {k_i}^2 \tag{28}$$

$$k_X = k_R \cos\Theta \tag{29}$$

$$k_Y = k_R \sin\Theta. \tag{30}$$

In the above expressions, i is zero for the observation point in the free space and equal to 1 for the observation point in the dielectric. $\overline{G}_E^{ZX}$, $\overline{G}_E^{ZY}$, $\overline{G}_E^{ZZ}$, $\overline{G}_H^{ZX}$ and $\overline{G}_H^{ZY}$ are denoted as $\overline{\psi}_i$. $\overline{\psi}_i$ satisfies the wave equation in the spectral domain

$$\left(\frac{d^2}{dZ^2} - {u_i}^2\right)\overline{\psi}_i = \text{contribution of sources.} \tag{31}$$

The boundary conditions at the interface between the free space and dielectric are expressed as follows,

$$\alpha_0\overline{\psi}_0 = \alpha_1\overline{\psi}_1 \quad \text{and} \quad \frac{\partial\overline{\psi}_0}{\partial Z} = \frac{\partial\overline{\psi}_1}{\partial Z}, \quad \text{at } Z = h \tag{32}$$

where

$$\alpha_i = \begin{cases} \varepsilon_i & : \quad \overline{\psi}_i = \overline{G}_E^{ZT} \\ \mu_0 & : \quad \overline{\psi}_i = \overline{G}_H^{ZT} \end{cases} \qquad (i = 0, 1),$$

and at the interface between the dielectric and ground plane,

$$\overline{G}_H^{ZT} = 0 \quad \text{and} \quad \frac{\partial\overline{G}_E^{ZT}}{\partial Z} = 0, \qquad \text{at } Z = 0. \tag{33}$$

By applying the boundary conditions (32) and (33) and the radiation condition to the solutions of the wave equation (31), $\overline{G}_E^{ZT}$ and $\overline{G}_H^{ZT}$ are obtained. The components K_A^{ST} of the dyadic function $\overline{\overline{\mathbf{K}}}_A$ and Green's functions for the scalar potential G_U in the spatial domain are derived by applying the inverse Fourier transform to $\overline{K}_A^{ST}$ and $\overline{G}_U$. The inverse Fourier transform is defined as [1]

$$g(X, Y, Z) = \frac{1}{2\pi}\int_0^\infty k_R \int_0^{2\pi} \overline{g}(k_R, \Theta) \times \exp\{jk_R R\cos(\Theta - \Phi)\}d\Theta dk_R. \tag{34}$$

Consequently, K_A^{ST} and G_U are expressed by the following equations.

$$K_A^{XX} = K_A^{YY} = \frac{\mu_0}{2\pi}\int_0^\infty \frac{Q_1}{\Delta_H} J_0(k_R R)k_R dk_R \tag{35}$$

$$K_A^{ZX} = -\frac{\mu_0}{2\pi}\cos\Phi\int_0^\infty \left(\frac{Q_2}{\Delta_H} - \frac{Q_3}{\Delta_E}\right) J_1(k_R R)dk_R \tag{36}$$

$$K_A^{ZY} = -\frac{\mu_0}{2\pi}\sin\Phi\int_0^\infty \left(\frac{Q_2}{\Delta_H} - \frac{Q_3}{\Delta_E}\right) J_1(k_R R)dk_R \tag{37}$$

$$K_A^{XZ} = -\frac{\mu_0}{2\pi}\cos\Phi\int_0^\infty \left(\frac{Q_4}{\Delta_H} - \frac{Q_5}{\Delta_E}\right) J_1(k_R R)dk_R \tag{38}$$

$$K_A^{YZ} = -\frac{\mu_0}{2\pi}\sin\Phi\int_0^\infty \left(\frac{Q_4}{\Delta_H} - \frac{Q_5}{\Delta_E}\right) J_1(k_R R)dk_R \tag{39}$$

$$K_A^{ZZ} = \frac{\mu_0}{2\pi}\int_0^\infty \left(\frac{1}{\Delta_H}\frac{\partial Q_4}{\partial Z} - \frac{1}{\Delta_E}\frac{\partial Q_5}{\partial Z}\right)\frac{J_0(k_R R)}{k_R}dk_R - \frac{\mu_0}{2\pi}\int_0^\infty \frac{1}{\Delta_E}\frac{\partial Q_5}{\partial Z}\frac{k_R}{{u_i}^2}\frac{\varepsilon_{ri}}{\varepsilon_{rj}}J_0(k_R R)dk_R \tag{40}$$

$$G_U = -\frac{1}{2\pi\varepsilon_i}\int_0^\infty \left(\frac{1}{\Delta_H}\frac{\partial Q_2}{\partial Z}\frac{{k_i}^2}{{u_i}^2} + \frac{1}{\Delta_E}\frac{\partial Q_3}{\partial Z}\right) \times \frac{J_0(k_R R)}{k_R}dk_R \tag{41}$$

$$\Delta_E = \varepsilon_0 u_1 \sinh(u_1 h) + \varepsilon_1 u_0 \cosh(u_1 h) \tag{42}$$

$$\Delta_H = u_1 \cosh(u_1 h) + u_0 \sinh(u_1 h) \tag{43}$$

$$R = \sqrt{r^2 + r'^2 - 2rr'\cos(\phi - \phi')} \tag{44}$$

$$\sin\Phi = \frac{r' - r\cos(\phi - \phi')}{R} \tag{45}$$

$$\cos\Phi = \frac{r\sin(\phi - \phi')}{R} \tag{46}$$

where $J_l(k_R R)$ is Bessel function of order l and ε_{ri} and ε_{rj} are the relative dielectric constant at the observation and source points, respectively. The expressions of $Q_k(k = 1, 2, \ldots, 5)$ are different in the positions of the observation and source points (See Appendix).

By subtracting the quasi-static terms from the integrands of Eqs. (35)–(41), the remaining integrands decay faster for larger k_R [1], [3]. The poles associated with the surface waves exist for $\Delta_E = 0$. The contributions from the poles are evaluated analytically by means of the residue calculus technique [1], [3].

4. Results and Discussion

The Eqs. (1)–(6) are applicable to only the MSAs with the thin patch conductor which can be analyzed using the cavity model. Therefore, the thickness $\delta_z \leqq 5.75 \times 10^{-4}\lambda_g$ of the patch conductor calculated in this paper is the range of validity of the cavity model [3]–[5]. λ_g is the wave length within the dielectric at the resonant frequency.

Figures 4(a) and (b) show the calculated $J_r^{U,L}$ and $J_\phi^{U,L}$ and Figs. 4(c) and (d) show the calculated J_z^S and J_ϕ^S at the resonant frequency (6.33 GHz), respectively. $J_r^{U,L} = 0$ and $J_z^S = 0$ at $\phi = 90°$ and $J_\phi^p(p = U, L, S) = 0$ at $\phi = 0°$. The numbers of expansion mode are chosen as $M = N = 3$. δ_z is $5.57 \times 10^{-4}\lambda_g$. In Figs. 4(a) and (b), the intensity of $\mathbf{J}^L$ is bigger than that of $\mathbf{J}^U$. This is due to the fact that $\mathbf{J}^L$ concentrates on the lower surface of the patch conductor because of the mutual coupling between the patch conductor and ground plane. The phase of $\mathbf{J}^L$ is nearly equal to that of $\mathbf{J}^U$. In Figs. 4(a) and (c), the intensity of J_z^S is very small compared with those of J_r^U and J_r^L. In Figs. 4(b) and (d), the singularities around the upper and lower edges of J_ϕ^S are almost equal to those of J_ϕ^U and J_ϕ^L, respectively.

Figure 5 shows the ratio of $|\mathbf{J}^U|$ to $|\mathbf{J}^L|$ at the center $(x = 0, y = 0)$ of the circular patch conductor for varying the thickness h of the dielectric substrate. The ratios are calculated at the resonant frequencies for each thickness of the dielectric substrate. The ratio of $|\mathbf{J}^U|$ to $|\mathbf{J}^L|$ decreases as the thickness of the dielectric substrate decreases. As mentioned above, this is due to the fact that the mutual coupling between the patch conductor and ground plane becomes stronger with decreasing the thickness of the dielectric substrate and the electric current concentrates on the lower surface of the patch conductor.

Figures 6(a) and (b) show the calculated input resistances and reactances. In these figures, the measured in-

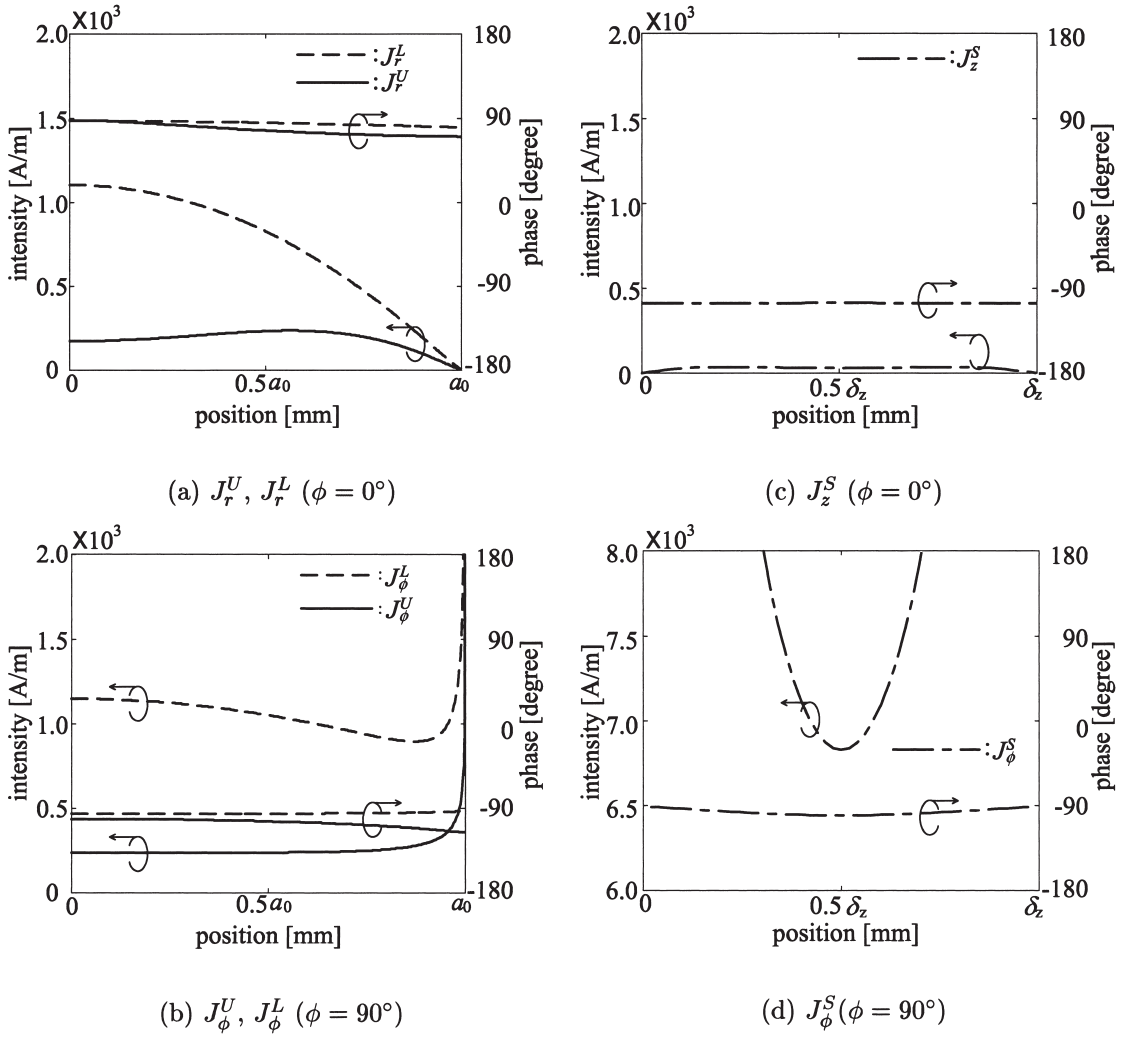

Fig. 4 Calculated electric current distributions (a_0=9.06 mm, d_0=6.0 mm, h=0.764 mm, ε_r=2.15, δ_z=0.018 mm, M=N=3, frequency=6.33 GHz).

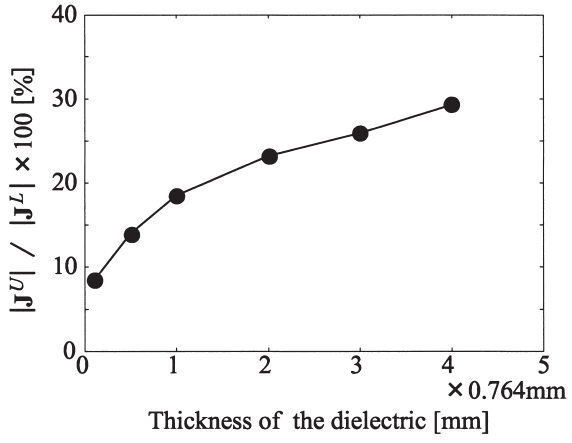

Fig. 5 Comparison of electric currents on the upper and lower surfaces of the patch conductor as function of the thickness of the dielectric (a_0=9.06 mm, d_0=6.0 mm, ε_r=2.15, δ_z=0.018 mm, M=N=3).

put impedance is also shown for comparison. The antenna is made of copper-clad Glass-fiber-PTFE. The input impedance Z_{in} is defined as the ratio of the voltage V_0 across the patch conductor and the ground plane to the feed point current I_0.

$$Z_{in} = \frac{V_0}{I_0} \tag{47}$$

$$V_0 = -\int_{-h}^{0} \mathbf{E}^f \cdot \mathbf{i}_z dz \tag{48}$$

where $\mathbf{E}^f$ is the electric field at the feed point ($r = d_0, \phi = 0°$). By using the vector and scalar potentials, the electric field $\mathbf{E}^f$ at the feed point is given as

$$\begin{aligned} \mathbf{E}^f &= \mathbf{E}^f(\mathbf{J}^U) + \mathbf{E}^f(\mathbf{J}^L) + \mathbf{E}^f(\mathbf{J}^S) \\ &= -j\omega\mathbf{A}^f(\mathbf{J}^U) - \nabla\phi_e^f(\mathbf{J}^U) \\ &\quad -j\omega\mathbf{A}^f(\mathbf{J}^L) - \nabla\phi_e^f(\mathbf{J}^L) \\ &\quad -j\omega\mathbf{A}^f(\mathbf{J}^S) - \nabla\phi_e^f(\mathbf{J}^S). \end{aligned} \tag{49}$$

The input impedance due to $\mathbf{J}^L$ is large compared with those of $\mathbf{J}^U$ and $\mathbf{J}^S$. $\mathbf{J}^U$ and $\mathbf{J}^S$ don't contribute to the input impedance. This is due to the following facts. The intensity

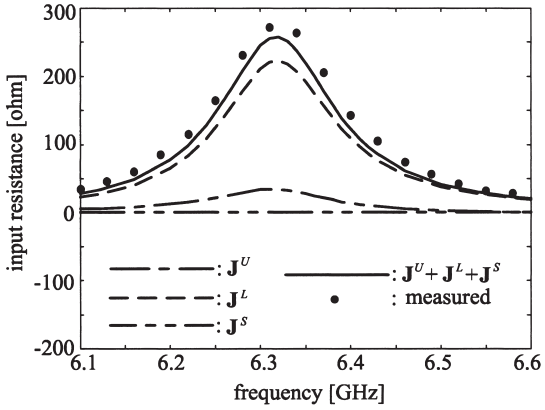

(a) Input resistances

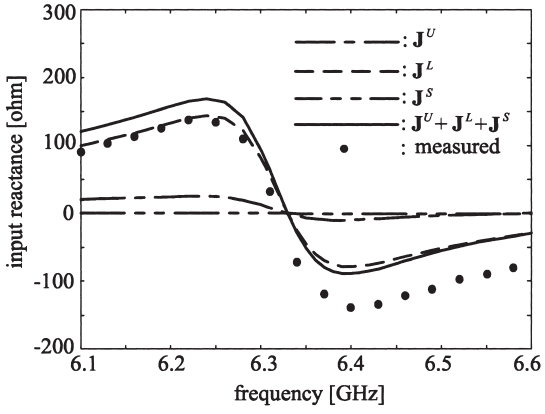

(b) Input reactances

Fig. 6 Input impedances of circular MSA (a_0=9.06 mm, d_0=6.0 mm, h=0.764 mm, ε_r=2.15, δ_z=0.018 mm, M=N=3).

of $\mathbf{J}^U$ is small compared with that of $\mathbf{J}^L$ and the thickness of the patch conductor δ_z is very small compared with the radius of the circular patch conductor a_0 ($\delta_z/a_0 \simeq 2.0\times10^{-3}$). The calculated input impedance due to the total electric currents ($\mathbf{J}^U + \mathbf{J}^L + \mathbf{J}^S$) agrees fairly well with the measured data.

5. Conclusion

The electric currents on the upper, lower and side surfaces of the patch conductor in the circular MSA have been calculated by the integral equation method and the characteristic between the electric currents on the upper and lower surfaces has been compared. The integral equations are derived from the boundary condition on the upper, lower and side surfaces of the patch conductor. The electric fields on the upper, lower and side surfaces of the patch conductor are derived by using Green's functions in the layered medium due to the horizontal and vertical electric dipoles on those surfaces. Green's functions in the spectral domain produced by the horizontal and vertical electric dipoles on the upper, lower and side surfaces of the patch conductor are derived by the boundary conditions at the interfaces between the free space, dielectric and ground plane and the radiation condition.

Since the real patch conductor is very thin, the electric currents on the surfaces of the patch conductor are assumed to follow closely the behavior of the corresponding eigenmode within the cavity. Moreover, in the expressions of the electric current, the edge condition of the metallic 90° corner is used. The calculated electric current on the lower surface is much bigger than that on the upper surface. Moreover, the ratio of the electric current on the upper surface to that on the lower surface at the center of the circular patch conductor decreases as the thickness of the dielectric substrate decreases. This is due to the fact that the electric current concentrates on the lower surface of the patch conductor because the mutual coupling between the patch conductor and ground plane becomes stronger as the thickness of the dielectric substrate decreases.

The input impedance of the MSA due to the electric current on the lower surface is bigger than those due to the electric currents on the upper and side surfaces. The input impedance of the MSA depends on the electric current on the lower surface.

References

[1] J.R. Mosig, "Integral equation technique," in Numerical techniques for microwave and millimeter-wave passive structures, ed. T. Itoh, pp.133–213, John Wiley & Sons, New York, 1989.

[2] K. Araki and T. Itoh, "Hankel transform domain analysis of open circular microstrip radiating structures," IEEE Trans. Antennas Propag., vol.AP-29, no.1, pp.84–89, Jan. 1981.

[3] T. Fujimoto, K. Tanaka, and M. Taguchi, "Wall admittance of a circular microstrip antenna," IEICE Trans. Commun., vol.E82-B, no.5, pp.760–767, May 1999.

[4] T. Fujimoto, K. Tanaka, and M. Taguchi, "Analysis of elliptical microstrip antennas with and without a circular slot," IEICE Trans. Commun., vol.E83-B, no.2, pp.386–393, Feb. 2000.

[5] T. Fujimoto, K. Tanaka, and M. Taguchi, "Analytical method for a circularly polarized rectangular microstrip antenna," IEE Proc. Microw. Antennas Propag., vol.148, no.2, pp.85–90, April 2001.

[6] K.A. Michalski, "On the scalar potential of a point charge associated with a time-harmonic dipole in a layered medium," IEEE Trans. Antennas Propag., vol.35, no.11, pp.1299–1301, Nov. 1987.

[7] K.A. Michalski and D. Zheng, "Electromagnetic scattering and radiation by surfaces of arbitrary shape in layered media, Part I: Theory," IEEE Trans. Antennas Propag., vol.38, no.3, pp.335–344, March 1990.

[8] J.V. Bladel, "Field singularities at metal-dielectric wedges," IEEE Trans. Antennas Propag., vol.33, no.4, pp.450–455, April 1985.

Appendix: Spectral Domain Green's Functions for the Vector and Scalar Potentials and Correction Term

Green's functions in the spectral domain $\overline{G}_A^{XX}$, $\overline{G}_A^{ZX}$, $\overline{G}_A^{YY}$, $\overline{G}_A^{ZY}$, $\overline{G}_A^{ZZ}$ and $\overline{G}_U$ and the correction term $\overline{P}_Z$ are obtained by substituting $\overline{G}_E^{ZT}(T = X, Y, Z)$, $\overline{G}_H^{ZT}(T = X, Y)$ into Eqs. (22)–(27).

$$\overline{G}_A^{XX} = \overline{G}_A^{YY} = \frac{\mu_0}{2\pi}\frac{Q_1}{\Delta_H} \tag{A·1}$$

$$\overline{G}_A^{ZX} = \frac{j\mu_0 k_X}{2\pi {k_R}^2}\left(\frac{Q_2}{\Delta_H} - \frac{Q_3}{\Delta_E}\right) \tag{A·2}$$

$$\overline{G}_A^{ZY} = \frac{j\mu_0 k_Y}{2\pi {k_R}^2}\left(\frac{Q_2}{\Delta_H} - \frac{Q_3}{\Delta_E}\right) \tag{A·3}$$

$$\overline{G}_A^{ZZ} = -\frac{\mu_0}{2\pi {u_i}^2}\frac{1}{\Delta_E}\frac{\partial Q_5}{\partial Z}\frac{\varepsilon_{ri}}{\varepsilon_{rj}} \tag{A·4}$$

$$\overline{P}_Z = \frac{\mu_0}{2\pi {k_R}^2}\left(\frac{Q_4}{\Delta_H} - \frac{Q_5}{\Delta_E}\right) \tag{A·5}$$

$$\overline{G}_U = -\frac{1}{2\pi\varepsilon_i {k_R}^2}\left(\frac{1}{\Delta_H}\frac{\partial Q_2}{\partial Z}\frac{{k_i}^2}{{u_i}^2} + \frac{1}{\Delta_E}\frac{\partial Q_3}{\partial Z}\right) \tag{A·6}$$

In the case of the electric dipole in the dielectric and the observation point in the dielectric,

$$Q_1 = [u_1\cosh\{u_1(h-Z)\} + u_0\sinh\{u_1(h-Z)\}] \times \frac{\sinh(u_1 Z')}{u_1} \tag{A·7}$$

$$Q_2 = [u_0\cosh\{u_1(h-Z)\} + u_1\sinh\{u_1(h-Z)\}] \times \sinh(u_1 Z') \tag{A·8}$$

$$Q_3 = [\varepsilon_0 u_1\cosh\{u_1(h-Z)\} + \varepsilon_1 u_0\sinh\{u_1(h-Z)\}]\sinh(u_1 Z') \tag{A·9}$$

$$Q_4 = [u_1\cosh\{u_1(h-Z)\} + u_0\sinh\{u_1(h-Z)\}] \times \cosh(u_1 Z') \tag{A·10}$$

$$Q_5 = [\varepsilon_0 u_1\sinh\{u_1(h-Z)\} + \varepsilon_1 u_0\cosh\{u_1(h-Z)\}]\cosh(u_1 Z') \tag{A·11}$$

In the case of the electric dipole in the dielectric and the observation point in the free space,

$$Q_1 = [\cosh\{u_0(h-Z)\} + \sinh\{u_0(h-Z)\}] \times \sinh(u_1 Z') \tag{A·12}$$

$$Q_2 = [\cosh\{u_0(h-Z)\} + \sinh\{u_0(h-Z)\}] \times u_0\sinh(u_1 Z') \tag{A·13}$$

$$Q_3 = [\cosh\{u_0(h-Z)\} + \sinh\{u_0(h-Z)\}] \times \varepsilon_0 u_1\sinh(u_1 Z') \tag{A·14}$$

$$Q_4 = [\cosh\{u_0(h-Z)\} + \sinh\{u_0(h-Z)\}] \times u_1\cosh(u_1 Z') \tag{A·15}$$

$$Q_5 = [\cosh\{u_0(h-Z)\} + \sinh\{u_0(h-Z)\}] \times \varepsilon_1 u_0\cosh(u_1 Z') \tag{A·16}$$

In the case of the electric dipole in the free space and the observation point in the dielectric,

$$Q_1 = [\cosh\{u_0(h-Z')\} + \sinh\{u_0(h-Z')\}] \times \sinh(u_1 Z) \tag{A·17}$$

$$Q_2 = -[\cosh\{u_0(h-Z')\} + \sinh\{u_0(h-Z')\}] \times u_1\cosh(u_1 Z) \tag{A·18}$$

$$Q_3 = -[\cosh\{u_0(h-Z')\} + \sinh\{u_0(h-Z')\}] \times \varepsilon_1 u_0\cosh(u_1 Z) \tag{A·19}$$

$$Q_4 = -[\cosh\{u_0(h-Z')\} + \sinh\{u_0(h-Z')\}] \times u_0\sinh(u_1 Z) \tag{A·20}$$

$$Q_5 = -[\cosh\{u_0(h-Z')\} + \sinh\{u_0(h-Z')\}] \times \varepsilon_0 u_1\sinh(u_1 Z) \tag{A·21}$$

In the case of the electric dipole in the free space and the observation point in the free space,

$mZ' \leqq Z \leqq \infty$

$$Q_1 = \Big[\cosh\{u_0(Z-h)\} - \sinh\{u_0(Z-h)\}\Big] \times \Big[u_0\sinh(u_1 h)\cosh\{u_0(Z'-h)\} + u_1\cosh(u_1 h)\sinh\{u_0(Z'-h)\}\Big]\frac{1}{u_0} \tag{A·22}$$

$$Q_2 = \Big[\cosh\{u_0(Z-h)\} - \sinh\{u_0(Z-h)\}\Big] \times \Big[u_0\sinh(u_1 h)\cosh\{u_0(Z'-h)\} + u_1\cosh(u_1 h)\sinh\{u_0(Z'-h)\}\Big] \tag{A·23}$$

$$Q_3 = \Big[\cosh\{u_0(Z-h)\} - \sinh\{u_0(Z-h)\}\Big] \times \Big[\varepsilon_1 u_0\cosh(u_1 h)\sinh\{u_0(Z'-h)\} + \varepsilon_0 u_1\sinh(u_1 h)\cosh\{u_0(Z'-h)\}\Big] \tag{A·24}$$

$$Q_4 = \Big[\cosh\{u_0(Z-h)\} - \sinh\{u_0(Z-h)\}\Big] \times \Big[u_0\sinh(u_1 h)\sinh\{u_0(Z'-h)\} + u_1\cosh(u_1 h)\cosh\{u_0(Z'-h)\}\Big] \tag{A·25}$$

$$Q_5 = \Big[\cosh\{u_0(Z-h)\} - \sinh\{u_0(Z-h)\}\Big] \times \Big[\varepsilon_1 u_0\cosh(u_1 h)\cosh\{u_0(Z'-h)\} + \varepsilon_0 u_1\sinh(u_1 h)\sinh\{u_0(Z'-h)\}\Big] \tag{A·26}$$

$h \leqq Z \leqq Z'$

$$Q_1 = \Big[\cosh\{u_0(Z'-h)\} - \sinh\{u_0(Z'-h)\}\Big] \times \Big[u_0\sinh(u_1 h)\cosh\{u_0(Z-h)\} + u_1\cosh(u_1 h)\sinh\{u_0(Z-h)\}\Big]\frac{1}{u_0} \tag{A·27}$$

$$Q_2 = -\Big[\cosh\{u_0(Z'-h)\} - \sinh\{u_0(Z'-h)\}\Big] \times \Big[u_0\sinh(u_1 h)\sinh\{u_0(Z-h)\} + u_1\cosh(u_1 h)\cosh\{u_0(Z-h)\}\Big] \tag{A·28}$$

$$Q_3 = -\Big[\cosh\{u_0(Z'-h)\} - \sinh\{u_0(Z'-h)\}\Big] \times \Big[\varepsilon_1 u_0\cosh(u_1 h)\cosh\{u_0(Z-h)\} + \varepsilon_0 u_1\sinh(u_1 h)\sinh\{u_0(Z-h)\}\Big] \tag{A·29}$$

$$Q_4 = -\Big[\cosh\{u_0(Z'-h)\} - \sinh\{u_0(Z'-h)\}\Big] \times \Big[u_0\sinh(u_1 h)\cosh\{u_0(Z-h)\} + u_1\cosh(u_1 h)\sinh\{u_0(Z-h)\}\Big] \tag{A·30}$$

$$Q_5 = -\Big[\cosh\{u_0(Z'-h)\} - \sinh\{u_0(Z'-h)\}\Big] \times \Big[\varepsilon_1 u_0\cosh(u_1 h)\sinh\{u_0(Z-h)\} + \varepsilon_0 u_1\sinh(u_1 h)\cosh\{u_0(Z-h)\}\Big] \tag{A·31}$$

Takafumi Fujimoto received his B.E. and M.E. degrees from Nagasaki University in 1992 and 1994, respectively, and a Dr. Eng. degree from Kyushu University in 2003. He is currently a Research Associate at Nagasaki University. His main interests are the analytical methods of microstrip antennas and the designing of microstrip antennas.

Kazumasa Tanaka received his B.S. M.S. and Dr.E. degrees in Electronic Communication Engineering, in 1965, 1967, and 1975, respectively, all from Kyushu University, Japan. Since 1981, he has been a professor at Nagasaki University. His main areas of interest are the diffraction-free beams, designing of optical filters and optical engineering. Dr. Tanaka is a member of the Japan Society of Applied Physics and the Optical Society of America.

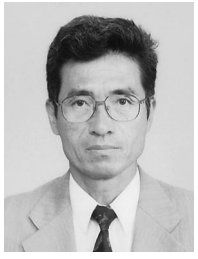

Mitsuo Taguchi received his B.E. and M.E. degrees from Saga University in 1975 and 1977, respectively, and a Dr.Eng. degree from Kyushu University in 1986. From 1977 to 1987, he was a Research Associate at Saga University. Since 1987 he has been an Associate Professor at Nagasaki University. In 1996 he was a Visiting Scholar in the Department of Electrical Engineering at the University of California, Los Angeles. His research interests are the active antennas, the microstrip antennas, and the linear antennas. He coauthored books, "Computational Electromagnetics," published by Baifukan, Tokyo, in 2003, "Foundations for Making Microwave Simulators," published by IEICE, Tokyo, in 2004, and "Modern Antenna Engineering," published by Sougou Denshi Publishing, Tokyo, in 2004. Dr. Taguchi is a member of the IEEE, the Applied Computational Electromagnetics Society, the Institute of Electrical Engineers of Japan and the Institute of Image Information and Television Engineers.